International Journal of Thermal Sciences 50 (2011) 169–177

Contents lists available at ScienceDirect

International Journal of Thermal Sciences

journal homepage: www.elsevier.com/locate/ijts

Experimental study on critical heat flux characteristics of R134a flow boiling in horizontal helically-coiled tubes

Chang-Nian Chen [a], Ji-Tian Han [a,*], Tien-Chien Jen [b], Li Shao [a], Wen-wen Chen [a]

[a] School of Energy and Power Engineering, Shandong University, Jinan, Shandong Province 250061, PR China
[b] Department of Mechanical Engineering, University of Wisconsin-Milwaukee, Milwaukee, WI 53201, USA

ARTICLE INFO

Article history:
Received 15 February 2010
Received in revised form
29 September 2010
Accepted 1 October 2010
Available online 5 November 2010

Keywords:
Critical heat flux
Horizontal helically-coiled tubes
R134a
Boiling heat transfer

ABSTRACT

Critical heat flux (CHF) experiments were performed to study the R134a CHF characteristics in horizontal helically-coiled tubes. The stainless steel test sections were heated uniformly, with tube inner diameters of 3.8–11 mm, coil diameters of 135–370 mm, helical pitches of 40–105 mm and heated lengths of 0.85–7.54 m. The experimental conditions are pressures of 0.30–1.10 MPa, mass fluxes of 60–480 kg $m^{-2} s^{-1}$, inlet qualities of −0.32–0.36 and heat fluxes of 6.0×10^3–9.0×10^4 W m^{-2}. It was found that the wall temperatures jumped abruptly once the CHF occurred. The CHF values decrease with increasing heated lengths, coil diameters and inner diameters, but the DNB (departure from nucleate boiling) CHF seems independent when length-to-diameter $L/d_i > 200$. The coil-to-diameter ratios are more important than length-to-diameter ratios for CHF in helically-coiled tubes, while the helical pitches have little effect on CHF. The CHF value increases greatly with increasing mass flux and decreases smoothly with increasing pressure. It decreases nearly linearly with increasing inlet and critical qualities, but it varies more acutely at $x_{cr} < 0.5$ than higher critical qualities. New correlations for R134a flow boiling CHF in horizontal helically-coiled tubes were developed for applications.

1. Introduction

Accurate prediction of critical heat flux (CHF) is very important for design and operation of various heated equipments such as evaporator, fuel cell cooling system, nuclear reactor, etc. It will cause a drastic reduction of heat transfer coefficient when CHF occurs. As heated uniformly, the wall temperature of boiling heat transfer tubes increases abruptly, causing the material of heated facilities to be sometimes destroyed, which is called boiling crisis [1]. For the past forty years, hundreds of experimental and mechanistic correlations for CHF have been developed with some satisfaction [1–12]. However, the mechanism of CHF is too complicated to be described by mathematical equations exactly, so most of the theoretical analysis results are limited [1–4]. It has been repeatedly shown previously that experimental investigations on CHF are utilizable to study characteristics of CHF in specific conditions and usually give good expectant results for applications [1,2].

According to mechanistic analysis, the CHF is roughly classified as two types, DNB (departure from nucleate boiling) CHF and dry-out CHF [2]. They are based on the different explanations for the trigger mechanism of CHF under different conditions. The DNB type CHF usually occurs where bubbles grow too fast to depart from heated surface due to very high heat flux. In this case, the temperature of bulk flow is lower than or equal to the saturated temperature. Actually, most of DNB CHF takes place in subcooling boiling conditions because of the existence of gas-phase (bubbles) between heated surface and cooling fluid, which awfully weakens the boiling heat transfer capability. The inducement for dry-out type CHF, just as its name implies, is mainly the avulsion and dry-out of liquid film caused by flow blowing and heat braising. The dry-out CHF usually occurs in annular flow pattern where the central core flow has a high velocity and can easily disperse the thin liquid film with help of the hot surface of tube wall. The DNB CHF works under much higher heat flux than the dry-out CHF, but both of them should be paid attention to in practical conditions related to the efficiency and security of operating heated equipment.

Efforts have been made to investigate CHF characteristics in straight tubes extensively, including horizontal and vertical straight tubes, with various fluids. Bowring [6] developed an accurate correlation for dry-out heat flux in round tube using water as working fluid over the pressure ranges of 0.7–12 MPa. His correlation was developed based on 3800 experimental data and had an error of 7% for CHF in water; Katto and Ohno [7] investigated on CHF of forced convective boiling in uniformly heated vertical tubes.

* Corresponding author. Tel./fax: +86 53188399060.
E-mail address: jthan@sdu.edu.cn (J.-T. Han).

1290-0729/$ – see front matter © 2010 Elsevier Masson SAS. All rights reserved.
doi:10.1016/j.ijthermalsci.2010.10.002

Nomenclature

A	heated area of the test section (m^2)
A', C'	coefficient in Eq. (5)
B_o	boiling number $B_o = \frac{q_{cr}}{G_i \gamma}$
C_p	thermal capacity ($J\,kg^{-1}\,K^{-1}$)
D	hydraulic diameter (m)
D_c	coil diameter (m)
D_n	Dean number $D_n = Re(\frac{D}{D_c})^{0.5}$
d_i	inner diameter of the test tube (m)
d_o	outer diameter of the test tube (m)
Fr	Froude number $Fr = \frac{G^2}{\rho^2 gD}$
G	mass flux ($kg\,m^{-2}\,s^{-1}$)
I	current (A)
k	thermal conductivity current ($W\,m^{-1}\,K^{-1}$)
L	heated length (m)
L_l	local length between calculated section and the inlet section (m)
N_d	liquid–gas density ratio $N_d = \frac{\rho_l}{\rho_g}$
P	pressure (MPa)
P_A	power value logged by Agilent software (W)
Pe	Peclet number $Pe = \frac{GDC_p}{k}$
P_e	power supplies for test section (W)
P_p	power supplies for preheating section (W)
P_t	helical pitch (m)
Q	heat flux ($W\,m^{-2}$)
q_{cr}	critical heat flux ($W\,m^{-2}$)
Re	Reynolds number $Re = \frac{GD}{\mu}$
$s1 - s8$	symbols of the test tube cross sections
T_0	temperature rise of an empty tube as same as the test section with increasing heat flux δq (K)
T_i	temperature at time i (°C)
T_{i-1}	temperature at time $i-1$ (°C)
T_w	wall temperature (°C)
U	voltage (V)
x_{cr}	critical quality
x_i	inlet quality
x_l	local quality
x_o	outlet quality
Y	combined parameter in Eq. (6)

Greek symbols

γ	latent heat of evaporation ($J\,kg^{-1}$)
Δh_i	inlet subcooling enthalpy ($J\,kg^{-1}$)
ΔT	wall superheat (K)
δq	increment of heat flux ($W\,m^{-2}$)
δT	temperature difference value defined according to the experimental conditions (K)
δT	error of T-type thermocouples (K)
λ	helical angle (°)
μ	dynamic viscosity (Pa s)
ρ	density ($kg\,m^{-3}$)

Subscripts

exp	experimental data
g	gas phase
l	liquid phase
pre	prediction data
ss	stainless steel

Their experiments covered nearly all the main characteristic regimes of CHF, but concerned only about vertical tubes; Shah [8] improved one general correlation for upstream flow CHF in vertical tubes comparing with Bowring and Katto correlations. His new correlation greatly agreed with CHF data of 23 fluids from 62 independent sources. Therefore, it was one of the most extensively used CHF correlations; Wong et al. [9] devised a new forecasting method for horizontal straight tubes. They established the models for the prediction of CHF in horizontal forced-convective flow from CHF in vertical flow using correction factors. The results gave a satisfying agreement with data; Kim et al. [10] conducted CHF experiments of water in vertical tubes under low pressure and low flow conditions (LPLF). They compared parametric trends under these special conditions with previous general understandings, considering the complex effects of system pressure and tube diameter; Groeneveld et al. [4] updated the CHF look-up table, which was a normalized data bank for vertical 8 mm water-cooled tube based on more than 30,000 data points; Sindhuja et al. [11] studied mixture R407c CHF in vertical tubes and compared the results with pure fluids, finding that the CHF characteristics change due to the mixture properties changing along the boiling length, but the results still showed lower CHF at higher pressure conditions as in the case of pure fluids. In addition, some efforts were contributed to investigate the CHF in nuclear reactor bundles [12–17].

For helically-coiled tubes, some studies concerned the flow boiling heat transfer and pressure drop characteristics [18–22]. A few researchers investigated the CHF characteristics in helical coils. Jensen and Bergles [23,24] performed a series of experimental studies on boiling heat transfer and CHF characteristics in helical coils using R113 as working fluid. They mainly emphasized on the effect of an outside heat flux tilt on the CHF and found that DNB CHF was degraded in coils relative to straight tubes, and the degradation increased with increasing the tube diameter-to-coil diameter ratio and the mass velocity, while dry-out CHF was enhanced and increased with increasing the tube diameter-to-coil diameter ratio. CHF initially increased with increasing mass velocity but began to decrease after a maximum value. Styrikovich et al. [25] presented their investigation on the temperature regime of a helical coil with both upflow and downflow of a steam-water mixture. They found that CHF in coils was higher than in a vertical straight tube, while the temperature regime of the coil tube in the post-dryout region was less severe. Jayanti and Berthoud [26] conducted an experiment about high-quality dryout in helical coils. They analyzed the influence of pressure, coil diameter, mass flux and heat flux on CHF and firstly proposed the correlations for the related area. Ma et al. [27] also carried out a research on high-quality CHF characteristics in helically coiled tubes. They evaluated the “local condition hypothesis” based on experimental data and discussed the “film inversion” phenomenon in coils. Zhang et al. [28] studied the deterioration of vapor-water boiling heat transfer in a helically-coiled tube and collected 272 data points for look-up table. However, their database was based on a helically-coiled tube set vertically, which can not cover horizontal ones.

An overview of the previous work shows that studies were mainly related to CHF behaviors in straight tubes, or bundles concerned by nuclear reactor only. As a kind of heat transfer enhancement tube, the helically-coiled tube has been widely used for industry [18,20]. Compared to straight tube, it has merits of high heat transfer efficiency and compact structure. It has a greater heat transfer area than a straight tube in the same amount of space. This is especially true for applications in aircrafts and submarines,

which both need narrow space to operate and the tube should be placed horizontally with a lower gravity center. Because of the coiled structure, more attention should be paid to the CHF phenomenon to avoid burnout of the heat exchanger made of coils. However, investigations on CHF in such horizontal helically-coiled tubes are scarce. On the other hand, although water is usually employed for heat transfer in engineering field, low latent heat substance such as Freon is usually used for experiments due to the high pressure and temperature conditions of vapor-water system. Subsequently, the results can be applied to water according to CHF fluid to fluid modeling methods based on similarity theory [3,16,29]. But the CFCs ever used in the past have been banned by Montreal Protocol considering their inherent destruction to ozonosphere. Therefore, the purpose of this paper is to present the CHF characteristics in horizontal helically-coiled tubes and the effect on CHF of structural parameters of tubes and system variables using environment-friendly R134a as working fluid. This is the fundamental work for CHF fluid to fluid modeling applied to water data in horizontal helically-coiled tubes, and also a contribution to R134a CHF database in helical coils, which will be employed for look-up table in the future.

2. Experimental apparatus and procedure

2.1. Experimental circle loop

The experimental set-up consists of two circle loops, the working loop (R134a) and the cooling loop (30% $CaCl_2$-water solution), as shown in Fig. 1. It includes the following components: canned motor pump, Coriolis mass flowmeter, preheating/test sections, precision DC power supplies, condenser, refrigeration chilling unit, N_2-gas accumulator and data acquisition system. The working loop is designed for pressure of 1.6 MPa and temperature of 200 °C, preheating section power supply of 24 V × 300 A and test section power supply of 60 V × 500 A. The refrigeration chilling unit has a maximum output of 50,000 W.

2.2. Test sections and installation

All the thirteen test sections are made of stainless steel tubes (Grade SUS304), the structure parameter ranges of which are shown in Table 1. The test section was directly electrified by high current DC power supply to generate constant heat flux (ignoring resistance variation of metal material).

The temperatures of the bulk flow R134a at the inlets and outlets of the preheating and test sections are measured with 0.3 mm T-type sheathed thermocouples. The precision pressure sensors are set at the same positions as thermocouples in order to measure pressures accurately. The temperatures of outside wall are measured by 0.2 mm T-type thermocouples made of copper-constantan set along the test tube. Eight symmetrical positions of each coil of the helically-coiled tube, i.e. every quarter-coil, as s1-s8 indicated in Fig. 2, are selected as measuring sections where four thermocouples are set evenly around the circumferences, 0°, 90°, 180°and 270° as indicated in Fig. 2. A total of thirty-two thermocouples are set in every coil. The four positions of the same section (0°−270°) are named upside, offside, underside and front, respectively. The inlet and the outlet sections selected are both 5 mm away from the copper electrodes connected with DC power supplies. The test tubes are wrapped with PEF (Polyethylene chemical bridging highly foamed materials) for heat preservation, and metal clamps are installed to stop from distortion of the test tube. All the experimental signals are transmitted to Agilent 34980A data acquisition system for processing.

2.3. Experimental conditions and procedure

Table 2 summarizes the condition ranges of a total of ninety-eight experiments. The results of these experiments taken under

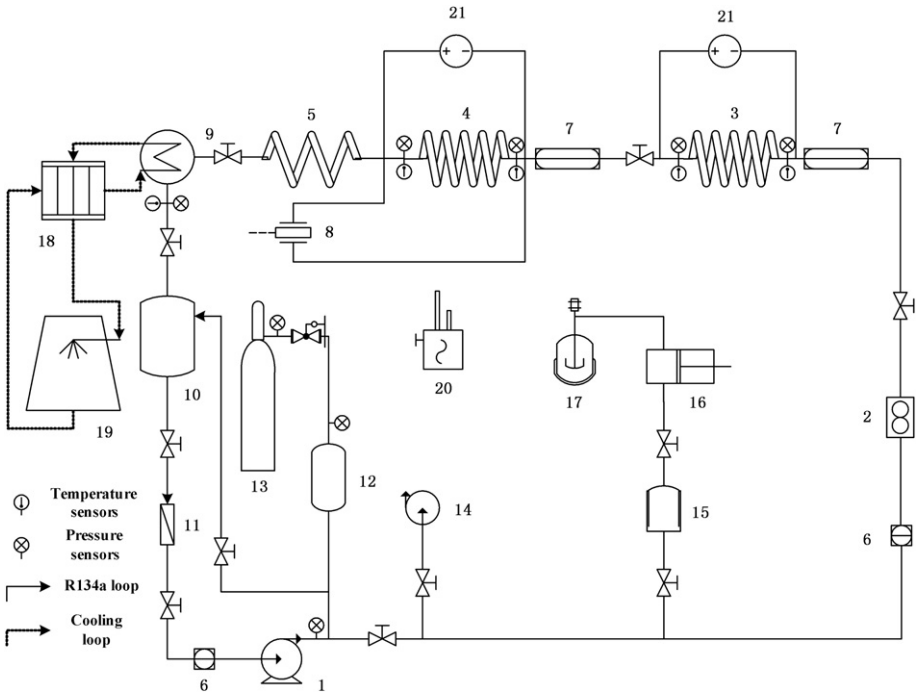

Fig. 1. Schematic diagram of the experimental circle loop. 1. motor pump, 2. Coriolis mass flowmeter, 3. preheating section, 4. test section, 5. flow pattern observing section, 6. sight glass, 7. visual section, 8. differential pressure gage, 9. condenser, 10. receiver tank, 11. dry-strainer, 12. accumulator, 13. N_2 gas tank, 14. vacuum pump, 15. buffer tank, 16. refrigerant pump, 17. refrigerant tank, 18. chilling unit, 19. cooling tower, 20. halogens leak detector, 21. DC power supply.

Table 1
Structure parameter ranges of test sections.

No.	Parameters	Ranges
1	Outer diameter d_o, mm	6, 10, 14
2	Inner diameter d_i, mm	3.8, 7.6, 8.4, 11
3	Coil diameter D_c, mm	135, 170, 210, 300, 370
4	Coil-diameter ratio D_c/d_i	17.8–78.9
5	Helical pitch P_t, mm	40, 45, 75, 105
6	Valid heated length L, mm	852.6–7541.2
7	Length-diameter ratio L/d_i	112–898

these conditions cover an extensively observation on CHF characteristics, including DNB CHF and dry-out CHF.

The procedures were conducted as follows. The helically-coiled tubes were placed horizontally and connected to the system with flange insulated. Before each experiment, heat balance testing was performed; the testing results showed that the average heat loss was no more than 5%. R134a from the receiver tank is circulated through the whole system by canned motor pump. The mass flux can be controlled by adjusting the speed of pump motor and control valves. The pressure is controlled by adjusting mass flux of cooling loop, power supply of preheating section and N_2-gas accumulator. When the pressure and mass flux of the system are stabilized to predetermined values, the inlet temperature is controlled by increasing or decreasing power supply to preheating section. The power supply to test section is increased rapidly at the beginning, then slowly at each step of about 50 W m^{-2} until CHF occurs. A method based on the event-driven Agilent BenchLink Data Logger Pro software was developed to determine the occurrence of CHF. CHF phenomena are considered to take place as long as any wall temperature T_i detected by thermocouples satisfies equation (1).

$$T_0 - (T_i - T_{i-1}) \le \delta T + \delta t$$
$$T_0 = \frac{4\delta q \cdot d_i}{\left(d_o^2 - d_i^2\right)\cdot \rho_{ss}\cdot C_{p,ss}} \quad (1)$$

Once the wall temperature reaches the limited value, the Agilent software gives an alarm and sends signal to cut off power supply within 0.1 s. The flow chart is described in Fig. 3.

3. Experimental results and discussion

3.1. Data reduction

In order to introduce the characteristics of CHF in horizontal helically-coiled tube and develop experimental correlations, critical heat flux q_{cr} (CHF value), inlet vapor quality x_i, local vapor quality x_l, outlet vapor quality x_o and critical vapor quality x_{cr} are needed. They are calculated with the following steps.

Table 2
Experimental condition ranges.

No.	Parameters	Ranges
1	Outlet pressure P, MPa	0.30–1.10
2	Mass fluxes G, kg m^{-2} s^{-1}	60–480
3	Inlet quality x_i	−0.32–0.36
4	Critical heat flux q_{cr}, W m^{-2}	6000–90,000

q_{cr} is derived from the arithmetic average of value q_{cr1} calculated by Agilent software and value q_{cr2} calculated by product of voltage U and current I logged in DC power supply.

$$q_{cr} = \frac{q_{cr1} + q_{cr2}}{2}$$
$$q_{cr1} = \frac{P_A}{A},\quad q_{cr2} = \frac{U\cdot I}{A} \quad (2)$$
$$A = \pi d_i L$$

Considering the heat losses of system within 5%, vapor qualities x_i, x_l, x_o and x_{cr} are evaluated by energy balance equation. The thermophysical properties of R134a are obtained from REFPROP Version 8.0 [30].

$$x_i = \frac{3.8P_p}{\pi\cdot G\cdot d_i^2\cdot\gamma} - \frac{\Delta h_i}{\gamma}$$
$$x_l = x_i + \frac{3.8P_e\cdot L_l}{\pi\cdot G\cdot d_i^2\gamma\cdot L}$$
$$x_o = x_i + \frac{3.8P_e}{\pi\cdot G\cdot d_i^2\cdot\gamma} \quad (3)$$

At the state of CHF, the thermodynamic equilibrium between gas phase and liquid phase near outlet of the test section is usually considered to be broken due to the extreme conditions [31]. However, calculation for real critical vapor quality is difficult to do. For the purpose of evaluating CHF, it is feasible to suppose critical vapor quality x_{cr} equals the thermodynamic equilibrium outlet vapor quality x_o.

3.2. Characteristics of wall temperature distribution

When the CHF occurs, the wall temperatures will rise up to high values rapidly. The temperature variety trend of different test sections under different experimental conditions is shown in Fig. 4(a)–(d).

The locations of the sudden rise in wall temperature along the heated length of test sections are shown in Fig. 4(a). The wall temperatures are the average values measured by thermocouples set around each section, and in the sections in which CHF occurs they are usually much higher than others. For different geometrical and system parameters, the wall temperatures show the same distribution regularity along the heated length of the test tubes. This

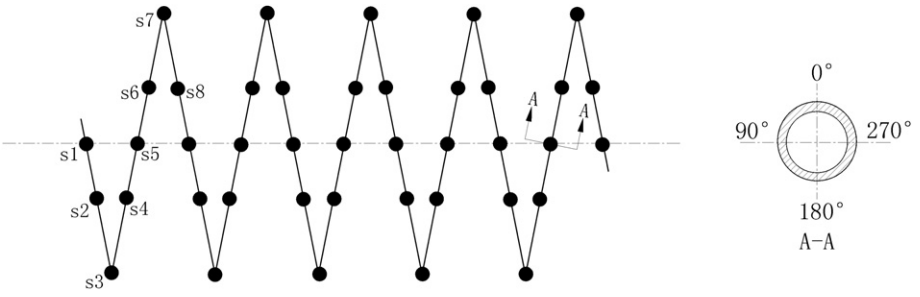

Fig. 2. Schematic diagram of the installation of thermocouples.

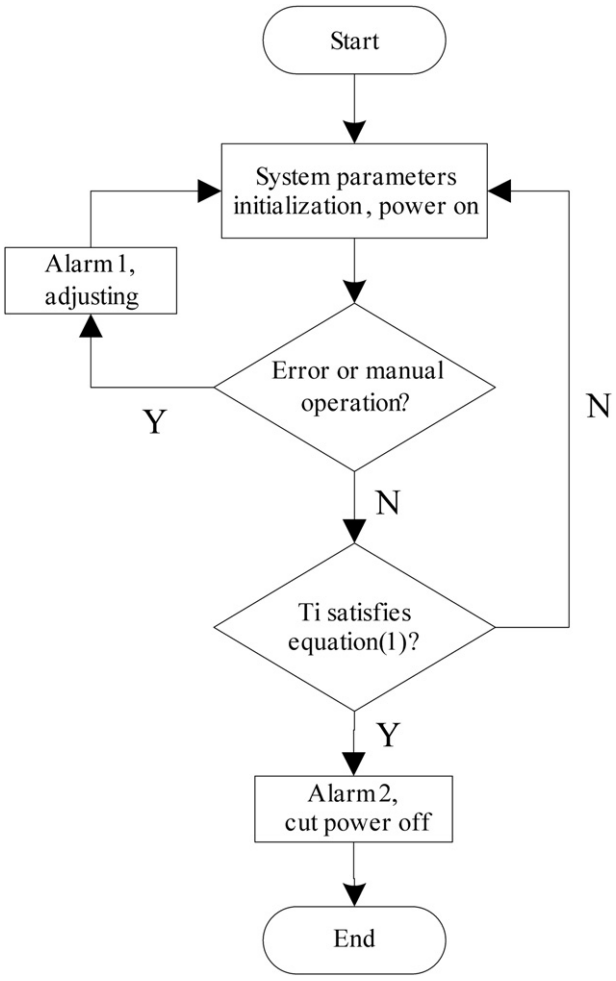

Fig. 3. Flow chart for determination of CHF occurrence.

is also shown plotted against the local vapor qualities along the heated length of tubes with kinds of different conditions in Fig. 4(b).

The characteristics of wall temperatures around the circumference of one section are shown in Fig. 4(c). Temperatures at all the four positions (0°–270°) give an obvious sudden rise with nearly a vertical slope. It seems not very clear to distinguish which position CHF firstly occurs at, but the temperatures at the front and offside (270° and 90°) are frequently higher than the other two sides, which agrees with the result of reference [32]. For further understanding, the sudden decline of wall temperatures as expected when power supplies are just cut off has been shown in Fig. 4(d). It seems that the temperatures at the upside and underside (0° and 180°) descend more quickly than the other two sides.

A typical flow boiling curve based on current experimental data has been plotted in Fig. 5 to show the CHF characteristics clearly. The whole flow boiling process can be divided into four regimes, viz. the single phase flow regime, the nucleate boiling regime, the transition boiling regime and the film boiling regime, as indicated *A*, *B*, *C* and *D* in Fig. 5. At the point of DNB, the heat transfer will be deteriorated drastically, and sometimes the flow boiling jumps into the regime *D*. In order to protect the heated equipment and for the sake of safety, the power will be cut off immediately once the CHF occurs as mentioned above. Although the data in regime *C* have been lost, a supposed dashed line and the dry-out CHF data still were plotted to complete the boiling curve, as shown in Fig. 5.

3.3. Parametric effect on CHF

An understanding of parametric effect on CHF is important for further development of accurate prediction theory. Previous work discussed parametric effect on CHF in straight round tubes extensively [2,6,8,33], but discussion in helically coiled tubes was scarce. This paper analyzes the effect of parameters on CHF based on experiments from two aspects, geometrical parameters and system parameters.

The CHF values vary with the geometrical parameters of helically coiled tubes as shown in Fig. 6(a), (b) and (c), including the effect of valid heated length, tube inner diameter, coil diameter, helical pitch (helical angle), length-to-diameter ratio and coil-to-diameter ratio.

The CHF decreases with increasing valid heated length for fixed d_i, G, P and x_i, while it increases a little with decreasing tube inner diameter for fixed L, G, P and x_i. The length-to-diameter ratio L/d_i has an more complex effect on CHF, and the CHF decreases with increasing L/d_i (<200) while this influence becomes unobvious when $L/d_i > 200$, especially for DNB type CHF, as shown in Fig. 6(a). The CHF decreases with increasing coil diameter for fixed d_i, G, P and x_i and increases little with decreasing tube inner diameter for fixed D_c, G, P and x_i. Compared with length-to-diameter ratio, the CHF decreases evidently with increasing the coil-to-diameter ratio D_c/d_i except for long tubes, as shown in Fig. 6(b). This suggests that D_c/d_i might be a more important parameter for CHF than L/d_i in helically coiled tubes. The helical pitch has a very little effect on CHF under various experimental conditions, as shown in Fig. 6(c). The effect of helical angle on CHF is also weak, because it is subject to coil diameter D_c and helical pitch P_t as follows.

$$\tan\lambda = \frac{P_t}{\pi \cdot D_c} \tag{4}$$

The CHF values vary with the system parameters as shown in Figs. 6 (a)–(c) and 7(a), (b), including the effect of mass flux, inlet vapor quality, outlet pressure and critical vapor quality.

The CHF value increase much with increasing mass fluxes for fix P and x_i, as shown in Fig. 6(a)–(c). And it has an approximately linear decline trend with increasing inlet vapor qualities at higher qualities under kinds of experimental conditions, but this influence becomes complex at high subcooling conditions, as shown in Fig. 7 (a). Outlet pressures do not have an obvious effect on CHF, and it seems like that CHF values decrease a little with increasing pressures for fixed G and x_i, as shown in Figs. 6 and 7. The CHF values decrease with increasing critical vapor qualities, as shown in Fig. 7 (b). It seems like that CHF values at low critical vapor qualities ($x_{cr} < 0.5$) vary acutely with x_{cr} than those at higher critical vapor qualities, which is usually related to DNB type CHF occurring at low critical vapor qualities [34].

3.4. Comparison with prediction results

Among existing correlations for CHF, Bowring [6] and Shah [8] correlations are more verified and convenient to use. Bowring correlation is expressed as follows:

$$q_{cr} = \frac{A' + 0.25D \cdot G \cdot \Delta h_i}{C' + L} \tag{5}$$

This correlation was derived from the following parameter ranges: $0.20 < P < 19.0$ MPa, $2.0 < D < 45.0$ mm, $150 < L < 3700$ mm and $136 < G < 18{,}600$ kg/m^2 s. Shah correlation is expressed as follows:

$$\begin{aligned} B_o &= f(L/D, Y, x_i) \\ Y &= Pe \cdot Fr^{0.4}\left(\mu_l/\mu_g\right)^{0.6} \end{aligned} \tag{6}$$

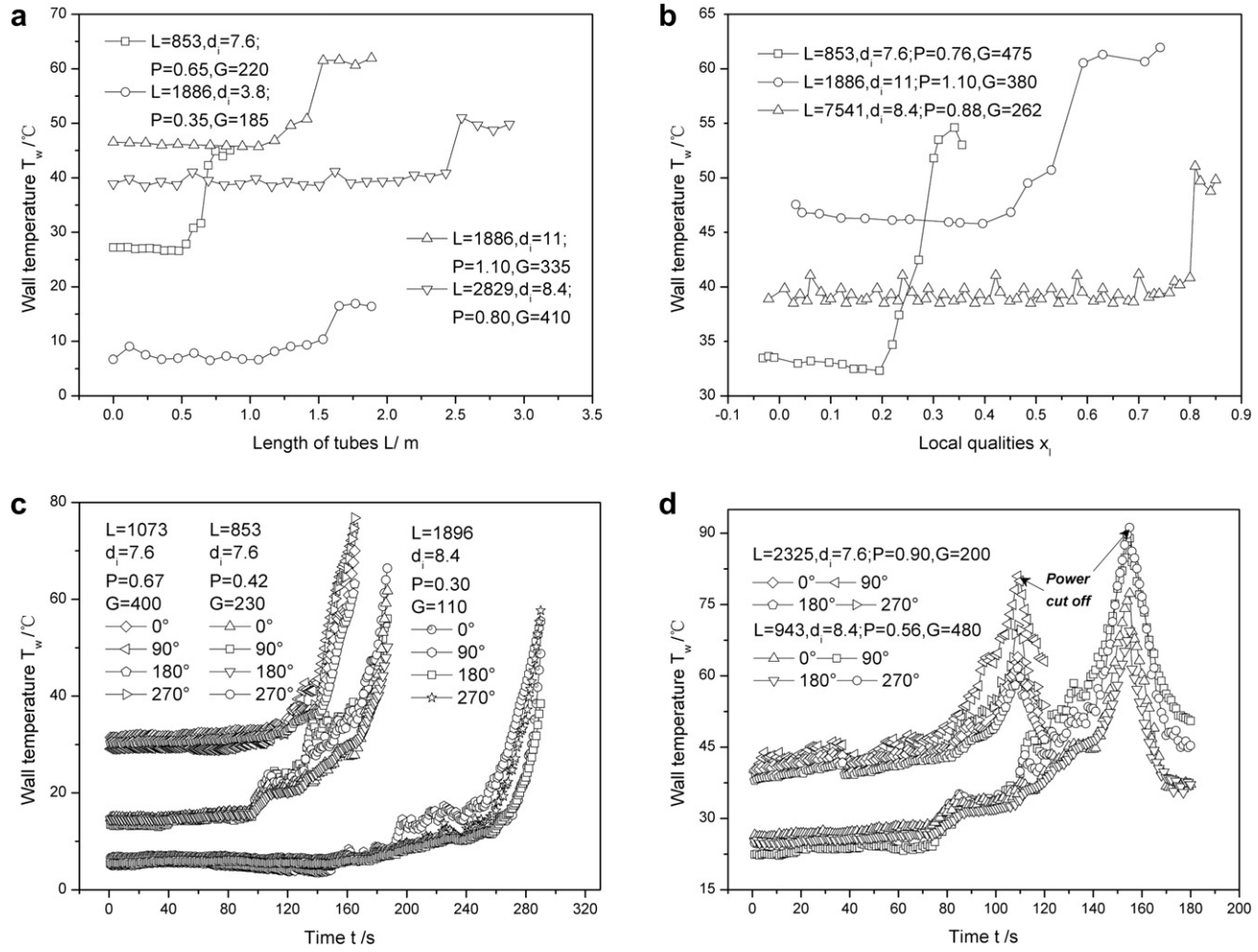

Fig. 4. (a) Characteristics of wall temperature distribution along the heated length of tubes. (b) Characteristics of wall temperature distribution with local qualities. (c) Characteristics of wall temperature distribution around the section circumference of tubes (power increasing). (d) Characteristics of wall temperature distribution around the section circumference of tubes (power cut off).

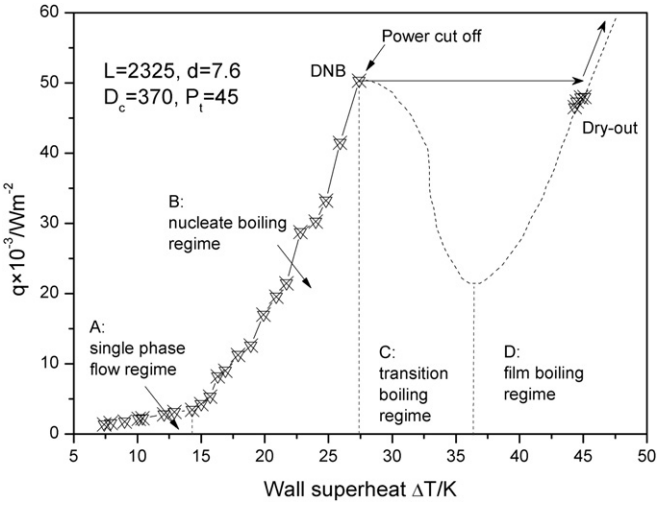

Fig. 5. Typical flow boiling curve based on current experimental data.

This correlation was applied widely for the parameter ranges with a mean error of 16%: reduced pressures of 0.0014–0.96, $1.30 < L/D < 940$, $0.315 < D < 37.5$ mm, and $3.90 < G < 29{,}051$ kg m^{-2} s^{-1}.

Experimental CHF data has been compared with the calculated results from Bowring and Shah correlations mentioned above at the same conditions, as shown in Fig. 8. It shows that the calculated values from the two correlations are dispersive much from the experimental results. Actually, both of them can give accurate CHF prediction in straight tube for water or R12, but are not suitable for R134a CHF in horizontal helically-coiled tubes under present experimental conditions.

New correlations for CHF in current experimental conditions were developed as follows. Considering the difference for dry-out type CHF and DNB type CHF based on experimental analysis, correlations are developed by inlet conditions and outlet conditions, respectively.

$$B_o = 8.071 \times 10^{-8} \mathrm{Re}^{2.12} D_n^{-2.5} N_d^{0.18} x_i^{-0.78}$$

$$B_o = 3.154 \times 10^{-7} \mathrm{Re}^{2.45} D_n^{-2.1} N_d^{0.46} x_o^{-0.25} \quad (7)$$

This correlation was applied to the following parameter ranges in horizontal helically-coiled tubes: $0.30 < P < 1.10$ MPa, $3.8 < D < 11$ mm, $850 < L < 7540$ mm, $135 < D_c < 370$ mm, $40 < P_t < 105$ mm and $60 < G < 480$ kg m^{-2} s^{-1}. The validity for CHF prediction shows that most of the experimental data fall in the region of ±20%, as indicated in Fig. 8.

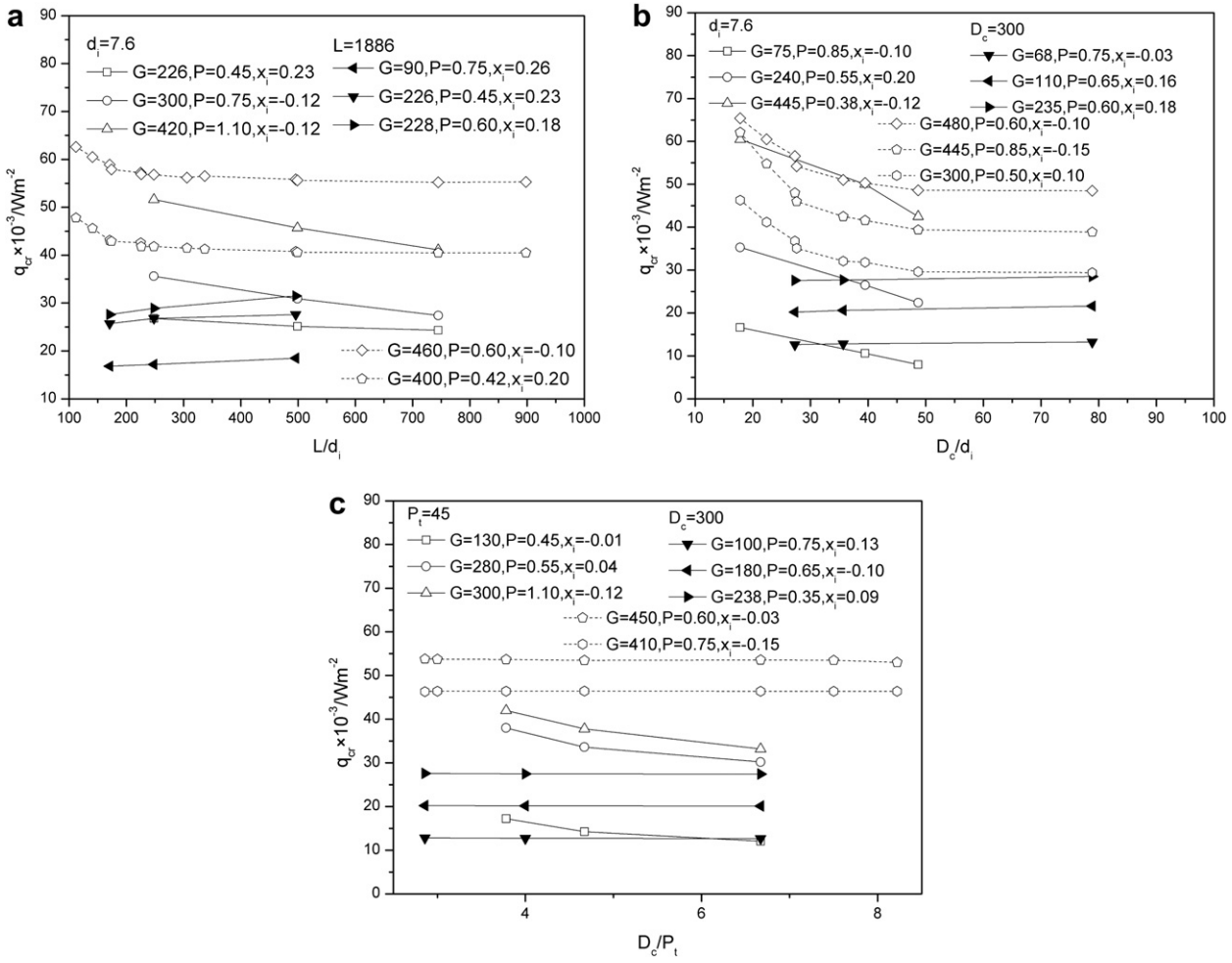

Fig. 6. (a) Effect of geometrical parameters on CHF with length-to-inner diameter ratios. (b) Effect of geometrical parameters on CHF with coil diameter-to-inner diameter ratios. (c) Effect of geometrical parameters on CHF with coil diameter-to-helical pitch ratios.

4. Experimental uncertainties

The directly measured parameters in experiments include length, temperature, pressure, mass flux, voltage and current. Based on the instructions of experimental equipments and verified data sheet, the maximum uncertainty in measuring length and inner diameter of test section is ±0.117% and ±0.53%, respectively; the maximum uncertainty in measuring temperature is ±0.49%; the maximum uncertainty in measuring pressure is ±1.3%; the maximum uncertainty in measuring mass flux is ±2.1%; the

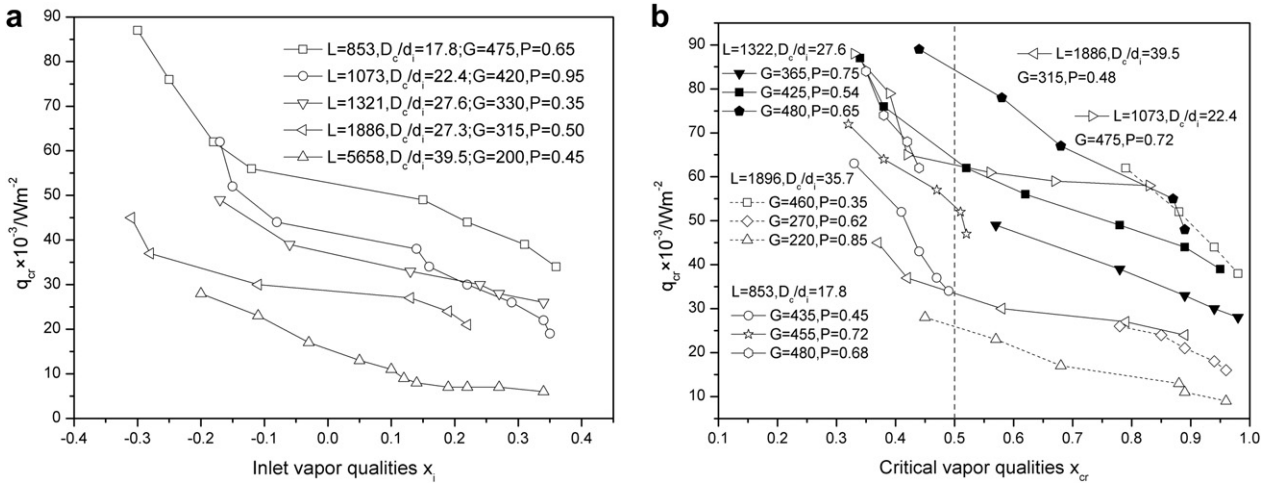

Fig. 7. (a) Effect of system parameters on CHF with inlet vapor qualities. (b) Effect of system parameters on CHF with critical vapor qualities.

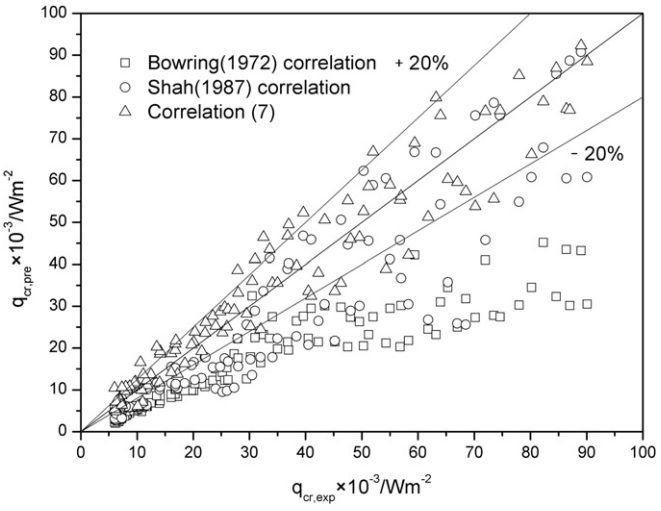

Fig. 8. Comparison of experimental data with correlations.

maximum uncertainty in measuring voltage and current is ±0.82% and ±2.2%, respectively. Thus, the maximum uncertainty in measuring the heated area of test tube and critical heat flux value is about ±0.54% and ±2.4%, respectively, according to Moffat's experimental error transfer procedure [35].

5. Conclusions

CHF experiments in horizontal helically-coiled tubes have been conducted using alternative refrigerant R134a.with thirteen test sections in wider parameter ranges. From analyzing the wall temperature distribution and parametric effect on CHF, the conclusions drawn are

(1) Once the CHF occurs, the wall temperatures jump abruptly. Those at the front and offside (270° and 90°) around the same section circumference are frequently higher than the other two sides. And those at the upside and underside (0° and 180°) descend more quickly than the other two sides when the power supplies are cut off. These characteristics seem to refer to the "film inversion" phenomenon in helical coils as reported by Hewitt and Jayanti [36] and Ma et al. [37]. When CHF occurs, the thinner liquid film forms at the front and offside due to interaction of both gravity and centrifugal force and can be easily torn out.

(2) Effect of length-to-diameter ratio on CHF becomes unobvious when $L/d_i > 200$, especially for DNB type CHF. This confirms that DNB type CHF relatively depends on the local conditions, knowing as the physical meanings of "local condition hypothesis" [38]. The coil-to-diameter ratio has a more evident effect on CHF than length-to-diameter ratio in helically coiled tubes. However, the helical pitch has little effect on CHF as illustrated in the text.

(3) The CHF values greatly increase with increasing mass fluxes; the CHF declining trend with increasing inlet vapor qualities becomes complex at high subcooling conditions. The CHF values at low critical vapor qualities ($x_{cr} < 0.5$) vary acutely with x_{cr} than those at higher critical vapor qualities; this maybe implies that CHF at low critical vapor quality shows its instability due to the special spiral structure of coils. In addition, pressures have an unobvious effect on CHF under present observation.

(4) Compared to experimental data, both of Bowring and Shah correlations are invalid for evaluating CHF in horizontal helically-coiled tubes. New correlations for current experimental conditions were developed for applications with errors of ±20%.

Acknowledgements

This work was supported by The National Natural Science Foundation of China (No.50776055) and Specialized Research Fund for the Doctoral Program of Higher Education (No.20090131110035). Dr. Tien-Chien Jen would also like to acknowledge partial financial support from EPA (USA) award RD 833357.

References

[1] Z.Q. Lu, Two-phase Flow and Boiling Heat Transfer. Tsinghua University Press, Beijing, China, 2002.
[2] J.G. Collier, J.R. Thome, Convective Boiling and Condensation, third ed. Clarendon Press, Oxford, England, 1994.
[3] S.Y. Ahmad, Fluid to fluid modeling of critical heat flux: a compensated distortion model, Int. J. Heat Mass Transfer 16 (1973) 641–662.
[4] D.C. Groeneveld, J.Q. Shan, A.Z. Vasic, L.K.H. Leung, Z.A. Durmaya, J. Yang, S.C. Cheng, A. Tanase, The 2006 CHF look-up table, Nucl. Eng. Des. 273 (2007) 1909–1922.
[5] N. Vaziri, A. Hojabri, A. Erfani, M. Monsefi, B. Nilforooshan, Critical heat flux prediction by using radial basis function and multilayer perceptron neural networks: a comparison study, Nucl. Eng. Des. 237 (2007) 377–385.
[6] R.W. Bowring, A simple but accurate round tube uniform heat flux, dry-out correlation over the pressure range, 0.7–12 MN/m^2 (100–2500 psia), Br. Report, AEEW-R789, Atomic Energy Establishment of Winfrith, Winfrith, U.K., 1972.
[7] Y. Katto, H. Ohno, An improved version of the generalized correlation of critical heat flux for the forced convective boiling in uniformly heated vertical tubes, Int. J. Heat Mass Transfer 27 (1984) 1641–1648.
[8] M.M. Shah, Improved general correlation for critical heat flux during upflow in uniformly heated vertical tubes, Int. J. Heat Fluid Flow 8 (1987) 325–335.
[9] Y.L. Wong, D.C. Groeneveld, S.C. Cheng, CHF prediction for horizontal tubes, Int. J. Multiphase Flow 16 (1990) 123–138.
[10] H.C. Kim, W.P. Bark, S.H. Chang, Critical heat flux of water in vertical round tubes at low pressure and low flow conditions, Nucl. Eng. Des. 199 (2000) 49–73.
[11] R. Sindhuja, A.R. Balakrishnan, S.S. Murthy, Critical heat flux of R-407c in upflow boiling in a vertical pipe, Appl. Therm. Eng. 28 (2008) 1058–1065.
[12] C.H. Lee, I. Mudawar, A mechanistic critical heat flux model for subcooled flow boiling based on local upflow conditions, Int. J. Multiphase Flow 14 (1988) 711–728.
[13] D.H. Hwang, W.P. Baek, S.H. Chang, Development of a bundle correction method and its application to predicting CHF in rod bundles, Nucl. Eng. Des. 139 (1993) 205–220.
[14] X. Cheng, U. Müller, Critical heat flux and turbulent mixing in hexagonal tight rod bundles, Int. J. Multiphase Flow 24 (1998) 1245–1263.
[15] I.L. Pioro, S.C. Cheng, A.Z. Vasic, R. Felisari, Some problems for bundle CHF prediction based on CHF measurements in simple flow geometries, Nucl. Eng. Des. 201 (2000) 189–207.
[16] J. Chen, J.R. Liao, B. Kuang, H. Zhao, Y.H. Yang, Fluid-to-fluid modeling of critical heat flux in 4 × 4 rod bundles, Nucl. Eng. Des. 232 (2004) 47–55.
[17] N.I. Kolev, Check of the 2005 look-up table for prediction of CHF in bundles, Nucl. Eng. Des. 237 (2007) 978–981.
[18] L.J. Guo, Dynamic characteristics of vapor/gas-liquid two phase flow in horizontal helically-coiled tubes, Ph.D. thesis, Xi'an Jiaotong University, Xi'an, China, 1989.
[19] R.C. Xin, A. Awwad, Z.F. Dong, M.A. Ebadian, An experimental study of single-phase and two-phase flow pressure drop in annular helicoidal pipes, Int. J. Heat Mass Transfer 18 (1997) 482–488.
[20] J.T. Han, C.X. Lin, M.A. Ebadian, Condensation heat transfer and pressure drop characteristics of R-134a in an annular helical pipe, Int. Commun. Heat Mass Transfer 32 (2005) 1307–1316.
[21] S. Wongwises, M. Polsongkram, Evaporation heat transfer and pressure drop of HFC-134a in a helically coiled concentric tube-in-tube heat exchanger, Int. J. Heat Mass Transfer 49 (2006) 658–670.
[22] L. Shao, J.T. Han, G.P. Su, J.H. Pan, Condensation heat transfer of R-134a in horizontal straight and helically coiled tube-in-tube heat exchangers, J. Hydrodyn. Ser. B. 19 (2007) 677–682.
[23] M.K. Jensen, Boiling heat transfer and critical heat flux in helical coils, Ph.D. thesis, Iowa State University of Science and Technology, Ames, USA, 1980.
[24] M.K. Jensen, A.E. Bergles, Critical heat flux in helical coils with a circumferential heat flux tilt toward the outside surface, Int. J. Heat Mass Transfer 25 (1982) 1383–1395.

[25] M.A. Styrikovich, V.S. Polonsky, V.V. Reshetov, Experimental investigation of the critical heat flux and post-dryout temperature regime of helical coils, Int. J. Heat Mass Transfer 27 (1984) 1245–1250.
[26] S. Jayanti, G. Berthoud, High-quality dryout in helical coils, Nucl. Eng. Des. 122 (1990) 105–118.
[27] W.M. Ma, M.Y. Zhang, X.J. Chen, High-quality critical heat flux in horizontally coiled tubes, J. Thermal Sci. 4 (1995) 205–211.
[28] W.B. Zhang, L. Zhao, X.J. Chen, D.B. Li, L.J. Guo, Investigation of boiling heat transfer deterioration of steam/liquid two-phase flow in a vertical helically coiled tube, J. Eng. Thermophys. 30 (2009) 1673–1676.
[29] I.L. Pioro, D.C. Groeneveld, S.C. Cheng, S.S. Doerffer, A.Z. Vasic, Yu.V. Antoshko, Comparison of CHF measurements in R-134a cooled tubes and the water CHF look-up table, Int. J. Heat Mass Transfer 44 (2001) 73–88.
[30] Nist, Refprop, Version 8.0, US Department of Commerce, USA, 2007.
[31] D.C. Grocheveld, G.G.J. Delorme, Prediction of thermal non-equilibrium in the post dry-out regime, Nucl. Eng. Des. 36 (1976) 17–26.
[32] Z.P. Feng, L.J. Guo, X.J. Chen, J.F. Sun, Dry-out characteristics of water in horizontal helically coiled tubes, J. Chem. Indus. Eng. 48 (1997) 180–184.
[33] S.K. Moon, W.P. Baek, S.H. Chang, Parametric trend analysis of the critical heat flux based on artificial neural networks, Nucl. Eng. Des. 163 (1996) 29–49.
[34] I.L. Pioro, D.C. Groeneveld, L.K.H. Leung, S.S. Doerffer, S.C. Cheng, Yu.V. Antoshko, Y. Guo, A.Z. Vasic, Comparison of CHF measurements in horizontal and vertical tubes cooled with R-134a, Int. J. Heat Mass Transfer 45 (2002) 4435–4450.
[35] R.J. Moffat, Describing the uncertainties in experimental results, Exp. Therm. Fluid. Sci. 1 (1988) 3–17.
[36] G.F. Hewitt, S. Jayanti, Prediction of film inversion in two-phase flow in coiled tubes, J. Fluid Mech. 236 (1992) 497–511.
[37] W.M. Ma, M.Y. Zhang, X.J. Chen, High-quality critical heat flux in horizontally coiled tubes, J. Therm. Sci. 4 (1995) 205–211.
[38] D.C. Groeneveld, On the definition of critical heat flux margin, Nucl. Eng. Des. 163 (1996) 245–247.